Discovery of an Allosteric Binding Site in Kinetoplastid Methionyl-tRNA Synthetase

Torrie, Leah S.; Robinson, David A.; Thomas, Michael G.; Hobrath, Judith V.; Shepherd, Sharon M.; Post, John M.

Published in:
ACS Infectious Diseases

DOI:
10.1021/acsinfecdis.9b00453

Publication date:
2020

ACS Infectious Diseases

pubs.acs.org/journal/aidcbc Article

Discovery of an Allosteric Binding Site in Kinetoplastid Methionyl-tRNA Synthetase

Leah S. Torrie, David A. Robinson, Michael G. Thomas, Judith V. Hobrath, Sharon M. Shepherd, John M. Post, Eun-Jung Ko, Rafael Alves Ferreira, Claire J. Mackenzie, Karolina Wrobel, Darren P. Edwards, Ian H. Gilbert, David W. Gray,* Alan H. Fairlamb, and Manu De Rycker*

Cite This: *ACS Infect. Dis.* 2020, 6, 1044−1057 Read Online

ACCESS | Metrics & More | Article Recommendations | Supporting Information

ABSTRACT: Methionyl-tRNA synthetase (MetRS) is a chemically validated drug target in kinetoplastid parasites *Trypanosoma brucei* and *Leishmania donovani*. To date, all kinetoplastid MetRS inhibitors described bind in a similar way to an expanded methionine pocket and an adjacent, auxiliary pocket. In the current study, we have identified a structurally novel class of inhibitors containing a 4,6-diamino-substituted pyrazolopyrimidine core (the MetRS02 series). Crystallographic studies revealed that MetRS02 compounds bind to an allosteric pocket in *L. major* MetRS not previously described, and enzymatic studies demonstrated a noncompetitive mode of inhibition. Homology modeling of the *Trypanosoma cruzi* MetRS enzyme revealed key differences in the allosteric pocket between the *T. cruzi* and *Leishmania* enzymes. These provide a likely explanation for the lower MetRS02 potencies that we observed for the *T. cruzi* enzyme compared to the *Leishmania* enzyme. The identification of a new series of MetRS inhibitors and the discovery of a new binding site in kinetoplastid MetRS enzymes provide a novel strategy in the search for new therapeutics for kinetoplastid diseases.

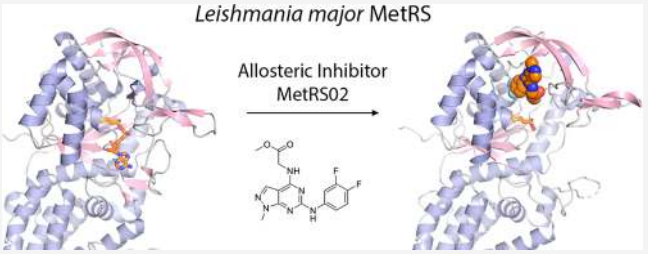

KEYWORDS: *Leishmania, kinetoplastid, methionyl-tRNA synthetase, drug discovery, allosteric, inhibitor*

Methionyl-tRNA synthetase (MetRS; EC 6.1.1.10) is a member of the aminoacyl-tRNA synthetase family of enzymes and plays a fundamental role in protein synthesis by catalyzing the production of methionyl-tRNA, a key molecule that binds AUG codons at the ribosome during translation, allowing the incorporation of methionine into nascent proteins. The production of methionyl-tRNA is a two-step procedure, with the first step resulting in the production of a methionyl-AMP intermediate and pyrophosphate and the second step producing methionyl-tRNA and AMP.

Due to the pivotal role that MetRS plays in protein synthesis, this enzyme has been described as a validated drug target in many disease-relevant organisms,[1−6] and several drug discovery programs against this target have been initiated.[1,2,4,7−14] In particular, MetRS has been successfully exploited as a target in Gram-positive bacteria with MetRS inhibitor CRS3123 having recently completed two phase I clinical trials for the treatment of *Clostridium difficile* infections (clinical trial identifiers NCT01551004 and NCT02106338).[13,15]

In addition to Gram-positive bacteria, MetRS has also been validated as a drug target in kinetoplastid parasites.[5,6,16−18] *Trypanosoma brucei subspecies*, *Leishmania species*, and *Trypanosoma cruzi* are the causative agents of human African trypanosomiasis, leishmaniasis, and Chagas disease, respectively. These neglected tropical diseases affect millions of people,[19] and new treatment options are urgently required due to limitations of the currently available therapies: high cost, host toxicity, and emerging drug resistance.[20] Consequently, identifying inhibitors of kinetoplastid MetRS provides a rational drug discovery strategy for these devastating diseases.

Previous high-throughput screening and drug discovery efforts have successfully identified potent inhibitors of both *T. brucei* MetRS (*Tb*MetRS) and *L. donovani* MetRS (*Ld*MetRS),[5,6,16−18,21−23] with well-characterized binding sites and modes of inhibition defined.[6,16−18,21,22,24,25] Interestingly, there is little chemical diversity found in the kinetoplastid MetRS inhibitors identified to date, with hit compounds sharing the same aminoquinolone core scaffold (compound series MetRS01) and binding to two well-characterized sites of the enzyme (the methionine pocket and an adjacent, auxiliary pocket)[6,21,22,24,25] that are highly conserved across all kinetoplastid MetRS enzymes.[26]

Received: November 22, 2019
Published: April 10, 2020

https://dx.doi.org/10.1021/acsinfecdis.9b00453
ACS Infect. Dis. 2020, 6, 1044−1057

Despite previous detailed characterization of the *Ld*MetRS aminoquinolone (MetRS01) inhibitor, DDD806905 (Figure 1A), this compound failed to translate into *in vivo* efficacy in a leishmaniasis animal model.[6] This was shown to be due to a combination of reasons: high protein binding, ionization of the compound, and accumulation of the compound in acidic compartments. Although DDD806905 failed to show *in vivo* efficacy, *Ld*MetRS remains an attractive *Leishmania* drug target requiring novel chemical start points.

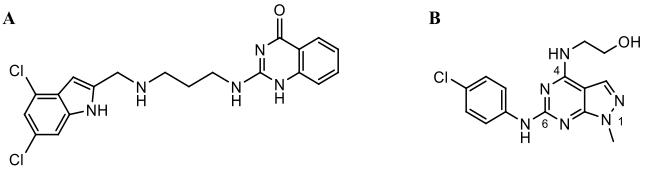

Figure 1. Structures of DDD806905 (MetRS01) and compound 1 (MetRS02). (A) DDD806905, a MetRS01 series inhibitor, was previously shown to inhibit *Ld*MetRS.[6] (B) Compound **1**, a MetRS02 series inhibitor, was identified as an *Ld*MetRS inhibitor in the current study (with the numbering of substituted positions on the 1*H*-pyrazolo[3,4-*d*]pyrimidine included).

In the current study, we describe the identification and characterization of a new series of *Ld*MetRS inhibitors that target a previously undefined, allosteric binding site in the enzyme. Further investigation of compounds from this chemical series shows that they have different inhibitory profiles against *Ld*MetRS and the *T. cruzi* MetRS enzyme (*Tc*MetRS), with crystallography and computational modeling used to rationalize these differences.

RESULTS

***Ld*MetRS: Hit Discovery.** In order to identify novel chemical starting points for an *Ld*MetRS drug discovery program, a new compound library screen was performed. All known MetRS inhibitors identified to date are competitive with respect to methionine; therefore, in an effort to identify compounds with an alternative mode of inhibition (with a bias toward ATP competitive compounds), a focused compound library, enhanced with ATP mimetics, was screened using the high-throughput *Ld*MetRS biochemical screening assay previously described.[6] This library of 6708 compounds was screened in single replicate at a concentration of 30 μM. To assess the robustness and reproducibility of the assay and the quality of the hit discovery campaign, various criteria were assessed following completion of the primary screen. These data reveal a high-quality screening campaign, with a mean robust Z'[27] of 0.82 ± 0.03 and a mean robust signal-to-background ratio of 2.48 ± 0.15. Hit compounds were identified by applying an arbitrary cutoff of 25% inhibition with 139 compounds from the focused ATP mimetic library meeting this criteria (2.1% hit rate) (Supporting Information Figure 1A,B). Hit compounds were cherry picked and retested as 10-point dose−response curves in the *Ld*MetRS assay to determine pIC_{50} (−log IC_{50} (M)) values (pIC_{50} range 4.0−5.1) (Supporting Information Figure 1C). During the subsequent chemistry assessment, representative compounds from the key chemical series were also tested in a counterscreen assay to determine whether there was any interference in the assay platform. None of the compounds tested showed inhibition in this counterscreen.

***Ld*MetRS: Key Series SAR.** Following the *Ld*MetRS high-throughput screen, compound **1** (Figure 1B and Table 1) was identified as the most potent representative of a series of compounds containing the 4,6-diamino-substituted pyrazolopyrimidine core (compound series MetRS02). This compound had moderate activity against *Ld*MetRS (pIC_{50} > 5), which was confirmed upon testing resynthesized material. A literature search indicated that pyrazolopyrimidines are a structurally novel class of MetRS inhibitors.

Table 1. Initial SAR from the 4,6-Diamine-Substituted Pyrazolopyrimidine Series Identified from an In-House Screen, with Modifications to the 6-Position (R^1)[a,b]

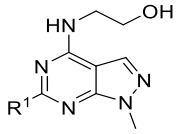

Compound No.	R^1	*Ld*MetRS pIC_{50}[a]	*Ld*MetRS Maximum % Inhibition Plateau	CHI LogD[b] (cLogP)
1	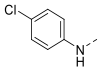	5.1	89.5	ND (1.91)
2	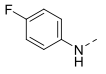	4.6	94.2	1.32 (1.52)
3	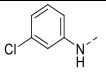	4.9	94.7	1.82 (1.84)
4	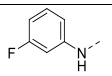	4.5	83.7	1.48 (1.44)
5	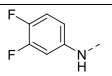	4.9	98.7	1.64 (1.67)
6	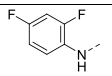	4.9	101.9	ND (1.67)
7	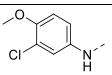	<4.0	N/A	ND (1.87)

[a]In all tables, data for active compounds are from $N \geq 2$ independent replicates. [b]CHI = chromatographic hydrophobicity index. cLogP = calculated log *P*.

From related analogues in the library screening set, the initial structure−activity relationship (SAR) (Table 1) suggested that small halogens were tolerated on the 6-anilino group (i.e., compounds **2**−**6**), whereas more polar substituents led to a loss of activity (i.e., compound **7**). Although little information could be gathered from the initial screening hits regarding the SAR around the 4-position, rapid SAR exploration of both the 4- and 6-positions was possible via sequential chlorodisplacements from commercially available 4,6-dichloro-1-methyl-1*H*-pyrazolo[3,4-*d*]pyrimidine as shown in Figure 2 and described in the Supporting Information.

The initial investigation of the SAR around the 6-position of the pyrazolopyrimidine (Table 2) focused on analogues which maintained or reduced cLogP and also explored the effect of increasing sp^3 character. This indicated that modification at this position was not well tolerated. Substitution of the aniline for aliphatic groups (i.e., compounds **8**−**11**) and methylation of the aniline nitrogen (i.e., compound **12**) led to a loss of activity, as

https://dx.doi.org/10.1021/acsinfecdis.9b00453
ACS Infect. Dis. 2020, 6, 1044−1057

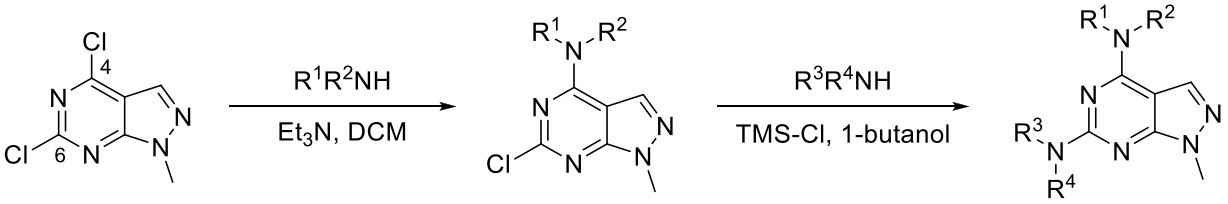

Figure 2. Generalized synthesis route to 1-methyl-1*H*-pyrazolo[3,4-*d*]pyrimidine-4,6-diamines.

Table 2. Modifications to the 6-Position (R^1)

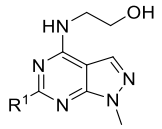

Compound No.	R^1	*Ld*MetRS pIC50	*Ld*MetRS Maximum % Inhibition	*Tc*MetRS pIC50	*Tc*MetRS Maximum % Inhibition	CHI LogD (cLogP)
8	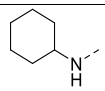	< 4.0	11.1	< 4.0	16.3	1.74 (1.81)
9	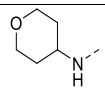	< 4.0	17.3	< 4.0	15.0	0.04 (0.65)
10		< 4.0	10.8	< 4.0	13.6	1.49 (1.17)
11		< 4.0	5.3	< 4.0	6.3	0.63 (0.98)
12	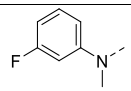	< 4.0	10.2	< 4.0	11.7	1.51 (1.73)
13	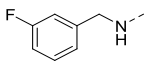	< 4.0	8.7	< 4.0	11.0	0.70 (1.57)
14	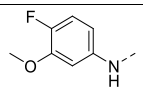	< 4.0	36.8	< 4.0	4.9	ND (1.49)
15	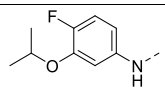	< 4.0	6.9	< 4.0	5.4	ND (2.36)
16	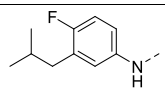	< 4.0	17.1	< 4.0	15.4	ND (3.03)

did homologation to the benzyl amine (i.e., compound **13**). Also, maintaining the *para*-fluoro substituent and introducing alternative *meta* substituents failed to improve the activity (i.e., compounds **14**−**16**).

Changes to the 4-position (Table 3) were made on the 3,4-difluoroanilino core, and this proved more successful. While aromatic groups were not tolerated (i.e., compound **17**), methylation of the 4-position NH led to a 5−10-fold increase in activity (i.e., compound **18** pIC_{50} = 5.2 vs compound **19** pIC_{50} = 6.0 and compound **6** pIC_{50} = 4.9 vs compound **20** pIC_{50} = 5.6) and methylation of the pendant hydroxyl group (i.e., compound **21**) also gave an increase in potency. Saturated amino-heterocycles (i.e., compounds **22** and **23**) were tolerated, and although a simple saturated cyclic amine (i.e., compound **24**) was inactive, an elaborated analogue (i.e., compound **25**) did retain activity possibly due to its potential to form a hydrogen

https://dx.doi.org/10.1021/acsinfecdis.9b00453
ACS Infect. Dis. 2020, 6, 1044−1057

Table 3. Modifications to the 4-Position (R^2)

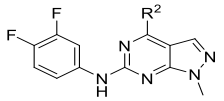

Compound No.	R^2	*Ld*MetRS pIC$_{50}$	*Ld*MetRS Maximum % Inhibition Plateau	*Tc*MetRS pIC$_{50}$	*Tc*MetRS Maximum % Inhibition Plateau	Aqueous Solubility (μM)	CHI LogD (cLogP)
17		< 4.0	N/A	< 4.0	N/A	0.38	3.82 (3.54)
18		5.2	98.7	<4.0	N/A	58.0	2.31 (2.17)
19		6.0	48.9	<4.0	N/A	4.8	2.88 (2.44)
20		5.6	69.9	< 4.0	N/A	2.4	1.99 (1.85)
21		5.2	99.7	<4.0	N/A	23.3	2.49 (2.27)
22		5.4	61.0	< 4.0	N/A	N/D	2.50 (2.92)
23		5.1	65.4	< 4.0	N/A	0.59	2.45 (2.71)
24		<4.0	N/A	< 4.0	N/A	0.46	3.93 (3.33)
25	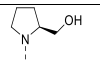	5.1	87.7	< 4.0	N/A	6.1	2.43 (2.41)
26		4.7	68.9	< 4.0	N/A	201	1.38 (1.36)
27		5.9	92.9	<4.0	N/A	5.5	2.17 (2.04)
28	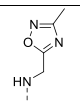	5.2	68.7	< 4.0	N/A	0.72	ND (2.60)
29		6.1	100.0	5.0	51.5	39.1	6.22 (3.11)
30	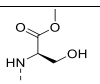	5.9	102.3	4.4	93.3	29.8	3.78 (1.80)
31	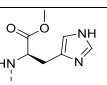	6.7	100.0	5.7	97.8	128	3.63 (2.33)
32		6.1	94.7	<4.0	N/A	N/D	4.91 (2.54)

bond with F339. While substitution with $CH_2CONHMe$ led to a 5-fold drop in potency (i.e., compound **26**), both the equivalent ester (i.e., compound **27**) and its 1,2,4-oxadiazole isostere (i.e., compound **28**) showed improved potency. To explore this

https://dx.doi.org/10.1021/acsinfecdis.9b00453
ACS Infect. Dis. 2020, 6, 1044−1057

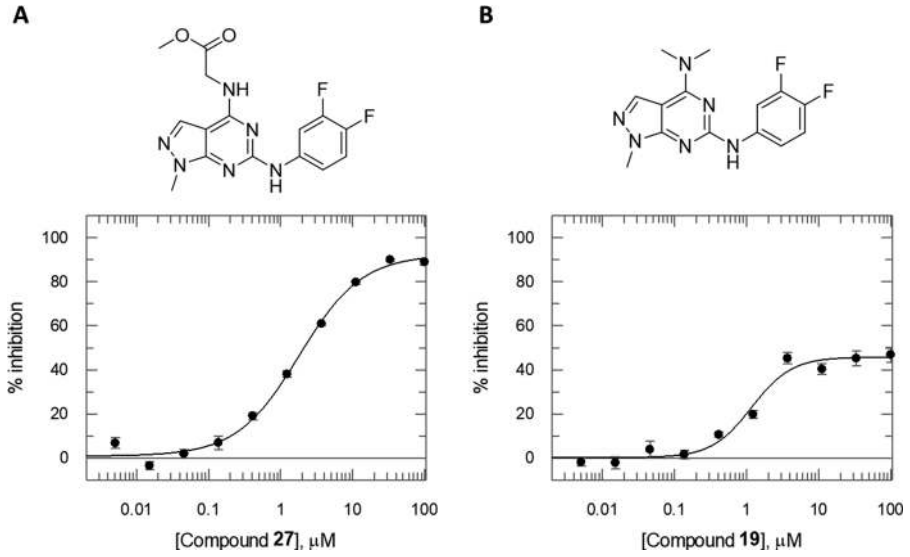

Figure 3. *Ld*MetRS compound **27** and Compound **19** pIC_{50} determinations. (A) Compound **27** and (B) compound **19** inhibit *Ld*MetRS with pIC_{50} values of 5.9 ± 0.2 (N = 19 independent replicates) and 6.0 ± 0.2 (N = 5 independent replicates), respectively, and with maximum % inhibition plateaus of 92.9 ± 3.7 and 48.9 ± 0.1, respectively, when screened using final substrate conditions of 50 μM methionine and 100 μM ATP. Representative dose−response curves are presented, with data points representing the mean % inhibition ± SD (n = 3 technical replicates).

further, a series of substituted aminoesters were introduced which led to a large improvement in activity, giving a series of analogues with pIC_{50} values above 5.9 (i.e., compounds **29**−**32**).

Despite the identification of compounds with submicromolar potencies against *Ld*MetRS, it was interesting to note that the compounds returned a variety of maximum % inhibition plateaus (Tables 1 and 3), with only a small number of compounds showing full inhibition of the enzyme. The partial inhibition profiles of the MetRS02 series are typified by two compounds: compound **27** (pIC_{50} 5.9 ± 0.2; maximum % inhibition 92.9 ± 3.7% (N = 19)) and compound **19** (pIC_{50} 6.0 ± 0.2; maximum % inhibition 48.9 ± 0.1% (N = 5)) (Figure 3).

MetRS02 Compound Solubility. A common explanation for partial inhibition profiles is low compound solubility. Aqueous compound solubility was therefore assessed and, for key representatives of the MetRS02 series, was generally found to be low (Table 3). Supporting Information Figure 2 shows the relationship between the maximum % inhibition plateau in the *Ld*MetRS dose−response curves and compound solubility, indicating that poor solubility is the most likely driver for the low plateaus observed in the *Ld*MetRS assay. Despite the poor solubility of many compounds in this series, we were able to develop compounds with good solubility and improved potency, resulting in full inhibition of the *Ld*MetRS enzyme (for example, compound **31**).

***Lm*MetRS: Binding Mode of Compound 27.** To determine the binding mode of the MetRS02 series of compounds, a protein ligand complex was obtained by co-crystallization of *Leishmania major* MetRS (*Lm*MetRS) with methionine and compound **27** bound (our most advanced compound at the time of the crystallography studies) (*Lm*MetRS:Met:MetRS02). As this series originated from an ATP mimetic compound library screen, we expected to see binding in an ATP competitive manner. Surprisingly, however, compound **27** was found to bind to a novel, allosteric ligand binding site (Figure 4).

In contrast to the binding mode of aminoquinolone inhibitors, which occupy both the methionine site and an enlarged ligand-stabilized auxiliary pocket, the MetRS02 ligand occupies a distinct site formed by the opening of the CP1 domain (Figure 4A). The CP1 domain is not opened to the same extent as observed for aminoquinolone (MetRS01) inhibitors, and methionine is found to be bound to the canonical methionine site, resulting in two distinct sites separated by the side chain of Trp443 (Figure 4B). The binding sites of MetRS01 and MetRS02 are mutually exclusive due to the movements of residues Tyr441, Val442, and Trp443, which form the base of the MetRS02 cavity. As a result, these residues cannot move to accommodate the MetRS01 chemotype, so the binding cavities are distinct (Figure 4D).

The MetRS02 site is created by a hinge movement of the CP1 domain from residues Lys327 and Glu372, resulting in an opening of 15°. The overall secondary structure of the CP1 domain is retained with fewer structural changes than observed for the conformational changes stabilized by the aminoquinolone inhibitors. The KISKS loop retains an open conformation due to the absence of ligands within the ATP binding site (Figure 4C). For productive catalysis to occur, both the CP1 domain and KISKS motif have to fully engage with substrate ATP; it is proposed that molecules from the MetRS02 series act as enzyme inhibitors by blocking CP1 domain movement, preventing the enzyme from forming the required catalytic conformation.

The MetRS02 binding site is largely hydrophobic in nature (Figure 4B), formed by side chains of Tyr328, Glu337, Ser338, Phe339, Phe414, Leu416, Ser417, Ile418, Tyr441, Trp443, Leu444, Leu447, Phe490, Tyr494, and Phe498. The difluorobenzyl group binds in a hydrophobic pocket formed by the side chains of Leu416, Ile418, Tyr441, Trp443, Leu444, Leu447, Phe490, Tyr494, and Phe498, while the pyrazolopyrimidine moiety stacks among Phe339, Phe414, and Tyr328.

Two H-bonds are formed between the pyrazolopyrimidine core and the backbone of Ser417; the one N lone pair interacts with the backbone NH, and the two amino NH groups interact with the backbone carbonyl. The pendant methyl acetate group carbonyl H-bonds to the backbone NH of Phe339 and enters a polar channel toward the active site.

https://dx.doi.org/10.1021/acsinfecdis.9b00453
ACS Infect. Dis. 2020, 6, 1044−1057

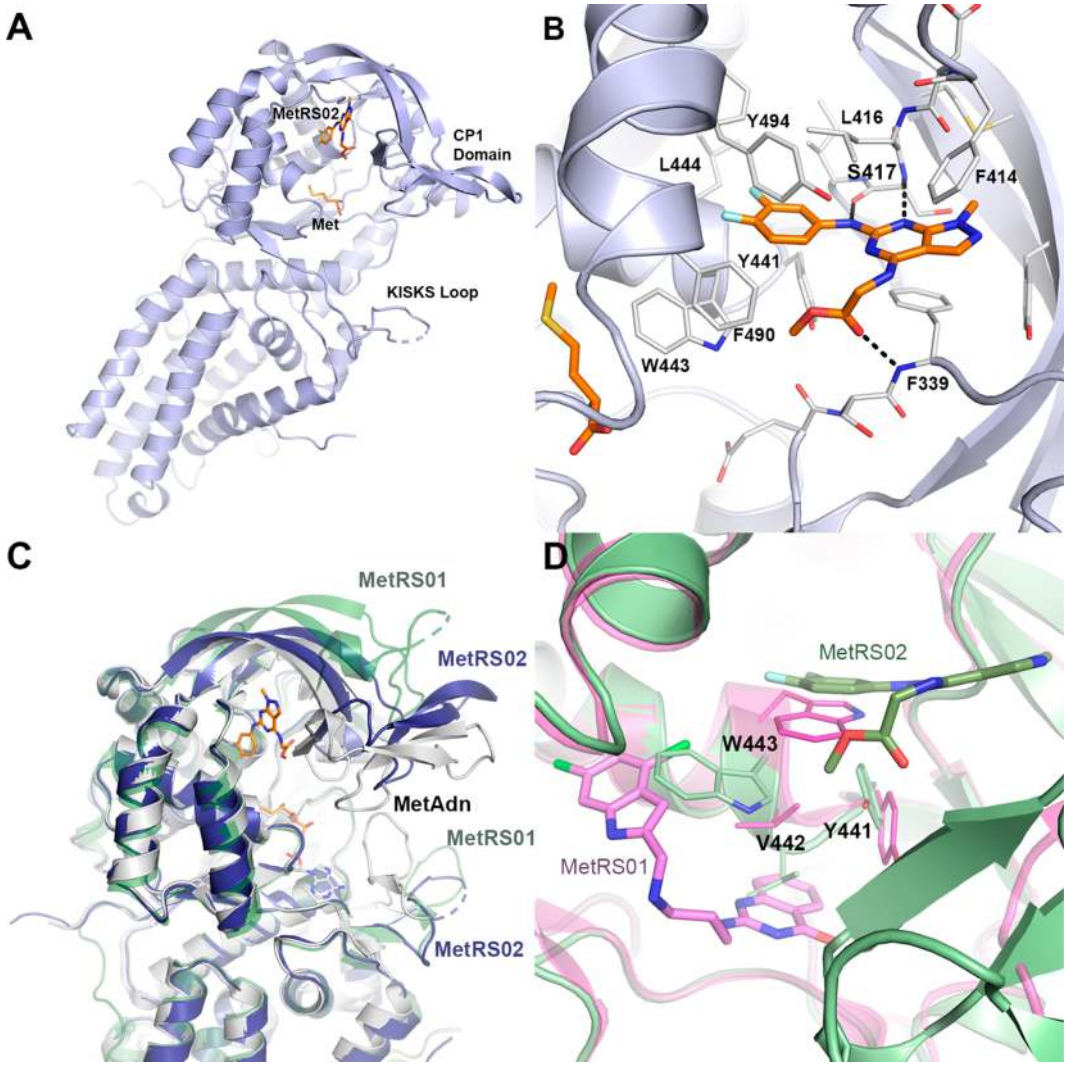

Figure 4. *Lm*MetRS compound **27** binding mode. (A) Binding mode of compound **27** (MetRS02) and methionine bound to *Lm*MetRS. Ligands are shown in a stick representation with C atoms colored gold. (B) Interactions formed between MetRS02 and *Lm*MetRS. H-bonds are shown as dashed lines, and key residues are labeled for clarity. (C) MetRS-ligand-stabilized conformational changes. *Lm*MetRS:MetAdn (PDB 3KFL), gray cartoon; *Lm*MetRS:Met:MetRS02, blue cartoon; and *Tb*MetRS:Met:MetRS01 (PDB 5NFH), green cartoon showing the movement of CP1 and KISKS domains. (D) Comparison of ligand binding sites. *Lm*MetRS:Met:MetRS02 C atoms, green; and *Tb*MetRS:Met:MetRS01 (PDB 5NFH) C atoms, magenta.

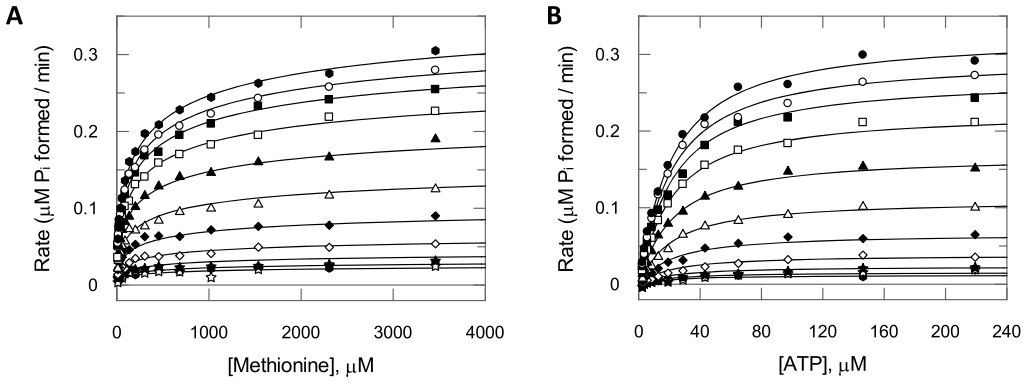

Figure 5. *Ld*MetRS compound **27** mode of inhibition. Rate versus (A) methionine or (B) ATP concentration plots for *Ld*MetRS in the presence of various concentrations of compound **27**. Data sets were globally fitted to the partial, cooperative, noncompetitive inhibition model (eq 7) with fit parameters reported in Table 4. (See also Supporting Information Figure 4, which highlights the quality of the data fit for the lower substrate concentrations tested.) For all data points, $n = 1$. In both panels, compound concentrations are 100 μM (closed hexagons), 50 μM (open stars), 25 μM (closed stars), 12.5 μM (open diamonds), 6.25 μM (closed diamonds), 3.13 μM (open triangles), 1.56 μM (closed triangles), 0.78 μM (open squares), 0.39 μM (closed squares), 0.2 μM (open circles), and 0 μM (closed circles).

https://dx.doi.org/10.1021/acsinfecdis.9b00453
ACS Infect. Dis. 2020, 6, 1044−1057

Table 4. Kinetic Parameters Describing Compound 27 and Compound 19 Modes of Inhibition[a]

compound	enzyme	substrate	K_i (μM)	β (fraction of activity remaining)	h (inhibitor Hill slope)	V_{max} (μM P_i formed/min)	K_s(μM)	n (substrate Hill slope)
27	*Ld*MetRS	methionine	2.06 ± 0.04	0.060 ± 0.005	1.05 ± 0.02	0.388 ± 0.009	327 ± 35	0.50 ± 0.01
		ATP	1.58 ± 0.04	0.027 ± 0.005	1.10 ± 0.02	0.324 ± 0.004	21.1 ± 0.6	1.07 ± 0.02[b]
	*Tc*MetRS	methionine	10.8 ± 0.7	0.65 ± 0.01	1.48 ± 0.11	0.429 ± 0.016	1340 ± 237	0.42 ± 0.01
		ATP	11.3 ± 1.2	0.48 ± 0.02	1.27 ± 0.14	0.287 ± 0.006	40.5 ± 2.0	1.07 ± 0.03[b]
19	*Ld*MetRS	methionine	1.22 ± 0.06	0.57 ± 0.01	1.65 ± 0.11	0.359 ± 0.009	313 ± 35	0.53 ± 0.02
		ATP	1.21 ± 0.06	0.55 ± 0.01	1.75 ± 0.12	0.292 ± 0.004	21.0 ± 0.74	1.03 ± 0.03[b]
	*Tc*MetRS	methionine	inactive	N/A	N/A	N/A	N/A	N/A
		ATP	inactive	N/A	N/A	N/A	N/A	N/A

[a]All data fits are to the partial, cooperative, noncompetitive mode of the inhibition model (eq 7). Data are presented as the parameter ± SE of fit to represent the goodness of fit of the data to eq 7. [b]As expected, the Hill value for ATP is close to 1. (No cooperativity is seen with this substrate.) Fixing this parameter to 1 for the ATP mode of inhibition experiments resulted in fit parameters in close agreement with those reported in the table above.

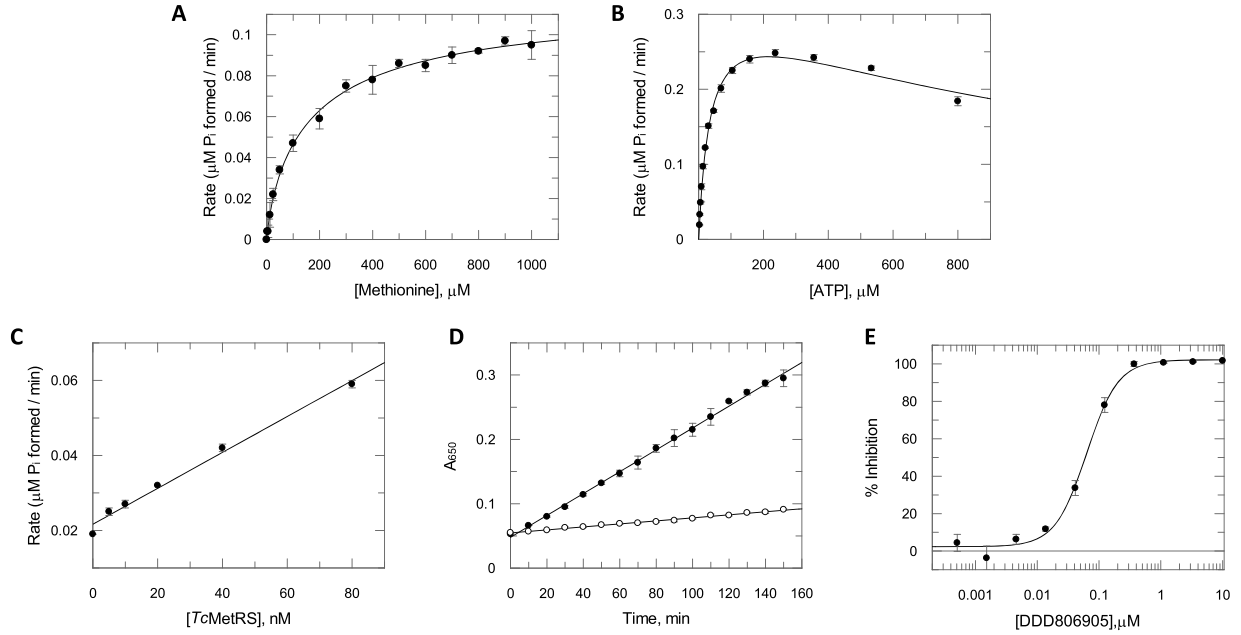

Figure 6. *Tc*MetRS assay development summary. (A) Methionine K_m^{app} determination in the presence of a saturating concentration of 350 μM ATP. Representative data are shown as the mean rate ± SD (n = 4 technical replicates) and were fitted to eq 1. (B) ATP K_m^{app} determination in the presence of a saturating concentration of 3 mM methionine. Representative data are shown as the mean rate ± SD (n = 4 technical replicates) and were fitted to eq 2. (C) Assay linearity with respect to enzyme concentration. Data are shown as the mean rate ± SD (n = 3 technical replicates). (D) Assay linearity with respect to time under the final assay screening conditions of 50 μM methionine and 100 μM ATP either with (closed circles) or without (open circles) the 80 nM *Tc*MetRS enzyme. Data are shown as mean A_{650} ± SD (n = 3 technical replicates). (E) Representative DDD806905 dose−response curve generated under final screening substrate conditions of 50 μM methionine and 100 μM ATP. Data are presented as the mean % inhibition ± SD (n = 3 technical replicates).

The observed binding mode of **27** to *Lm*MetRS provides a structural rationale for the SAR derived for the MetRS02 series in general (Tables 1−3). The hydrophobic nature of the difluorobenzyl pocket explains the distinct preference for aromatic substituents at the 6-position of the pyrazolo-pyrimidine core with a potency loss for molecules with aliphatic or polar moieties. The importance of the H-bond formed by the aniline NH with the protein backbone is highlighted by the loss of potency when methylated. The observed SAR for substitution at the 4-position shows a preference for an H-bond acceptor group as exemplified by the interaction between the ester carbonyl of **27** and the NH backbone of Phe339.

***Ld*MetRS: MetRS02 Series Mode of Inhibition.** In addition to the crystallographic information, enzymatic studies were also carried out on compounds from the MetRS02 series to determine their mode of inhibition. Preliminary data generated with compound **27** revealed no IC_{50} shifts when the methionine and ATP concentrations were increased from 50 μM each to 500 μM (Supporting Information Figure 3), suggesting that this inhibitor is not competitive with either substrate.

Subsequent full mode of inhibition studies with compounds from the MetRS02 series were more challenging due to the partial inhibition profiles of some compounds resulting in poor global fits to the standard competitive, uncompetitive, and noncompetitive inhibition models (eqs 3, 4, and 5, respectively). In addition, during the enzymatic characterization of methionine binding to *Ld*MetRS, a Hill slope of <1 was obtained (and was hypothesized to be due to conformational selection).[6] This low Hill slope is also not factored into the standard inhibition models described (eqs 3−5). New models with additional parameters to account for the partial inhibition and low methionine Hill slope were therefore required (eqs 6 and 7).

https://dx.doi.org/10.1021/acsinfecdis.9b00453
ACS Infect. Dis. 2020, 6, 1044−1057

Using these modified equations, the mode of inhibition of compound **27** was carried out by testing *Ld*MetRS enzyme activity under varying substrate concentrations at various inhibitor concentrations (Figure 5). The cooperative, non-competitive, partial inhibition model (eq 7) was confirmed as the best fit (using F-test analyses), with a noncompetitive mode of inhibition consistent with binding in an allosteric binding pocket. The returned fit parameters are shown in Table 4 and are presented with the standard error (SE) of the fit to eq 7. In most cases, the SE is <10% of the parameter value highlighting the excellent fit observed, with Supporting Information Figure 4 also demonstrating the high-quality fit even at low substrate concentrations.

Mode of inhibition studies for a second available compound from this series (compound **19**) confirmed that the non-competitive mode of inhibition model (eq 7) was the best fit to the data (Supporting Information Figure 5 and Table 4).

***Tc*MetRS: Assay Development.** The novel allosteric binding pocket and the noncompetitive inhibition profile seen with the MetRS02 series of compounds were unexpected given that this hit series came from a screen of a compound library enriched with ATP mimetics. As expected from the high degree of active site homology between the kinetoplastid MetRS enzymes, the previously described orthosteric MetRS01 series shows MetRS inhibition across kinetoplastid species. However, as the newly identified *Ld*MetRS inhibitors target an allosteric binding pocket not previously described, we were interested in investigating the activity of the MetRS02 compound series in another kinetoplastid MetRS enzyme. As Chagas disease is a key disease focus for our organization, MetRS from *Trypanosoma cruzi* was selected for further study.

A BIOMOL Green biochemical assay, comparable to that developed for *Ld*MetRS, was also developed for *Tc*MetRS, with Michaelis constants for the methionine and ATP substrates determined (Figure 6A,B) and assay linearity with respect to enzyme concentration and time assessed (Figure 6C,D).

The *Tc*MetRS apparent Michaelis constants for methionine and ATP were determined to be 212 μM (95% CI 139−324 μM; N = 3 independent replicates) (with a Hill slope of 0.63 ± 0.16) and 63 μM (95% CI 31−125 μM; N = 3 independent replicates) (with a substrate inhibition constant of 2080 μM (95% CI 1160−3740 μM)), respectively. These K_m^{app} values are highly comparable to those previously determined for the *Ld*MetRS enzyme (173 and 37 μM for methionine and ATP respectively).[6] In addition, the subunity Hill slope observed with methionine and the substrate inhibition observed with ATP match that seen in the *Ld*MetRS assay, suggesting that, kinetically, the two enzymes are very similar. For screening purposes, the *Tc*MetRS assay was configured to match the *Ld*MetRS assay, with subsaturating concentrations of 50 μM methionine and 100 μM ATP selected to ensure that the assay was not biased toward a particular inhibition modality. Using these assay conditions, the *Tc*MetRS assay was validated using previously described *Ld*MetRS inhibitor DDD806905. This MetRS01 compound was shown to inhibit the *Tc*MetRS enzyme with a pIC_{50} of 7.4 ± 0.1 (mean ± SD; N = 16 independent replicates (IC_{50} 38 nM)) (Figure 6E), which is comparable to the pIC_{50} of 7.0 (IC_{50} 94 nM) described for *Ld*MetRS.[6] However, on the basis of the enzyme concentration used in the biochemical assay (80 nM *Tc*MetRS) and the high Hill slopes determined in the IC_{50} fits (Hill slopes = 2.6 ± 0.3), it is highly likely that the tight binding limit of the *Tc*MetRS assay has been reached and the actual IC_{50} of DDD806905 is lower than recorded.

***Ld*MetRS versus TcMetRS Inhibitor Correlations.** Interestingly, screening key compounds from the MetRS02 series revealed that most compounds were inactive against *Tc*MetRS (defined as no compound concentration tested showing >50% inhibition, i.e., IC_{50} > 100 μM; pIC_{50} < 4.0) (Table 3). Further investigation of a larger panel of 201 compounds from this chemical series (available from an unrelated in-house project) shows a wide range of potencies against *Ld*MetRS (pIC_{50} range 4.0−6.7) and confirms the much lower potency against *Tc*MetRS (Figure 7). On the basis of the data for the more soluble and potent compounds (compounds **29**−**31**), compounds in this series are approximately 10-fold less potent against the *Tc*MetRS enzyme than against *Ld*MetRS.

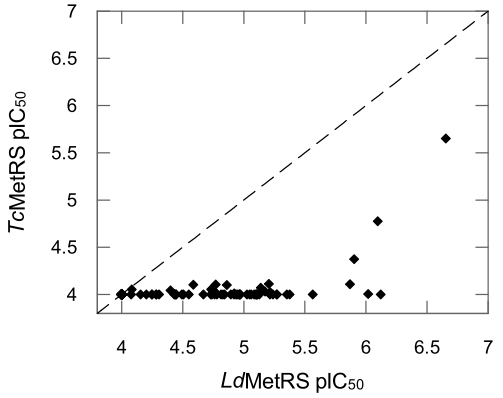

Figure 7. *Ld*MetRS versus *Tc*MetRS potency correlation. Correlation between mean *Ld*MetRS pIC_{50} and mean *Tc*MetRS pIC_{50}. Dashed line is a line of equipotence. Data points represent the mean pIC_{50} (N = 2 independent replicates).

While representative compound **27** returned a pIC_{50} < 4 in our *Tc*MetRS screening assay, it still showed some level of inhibition of the *Tc*MetRS enzyme, with a maximum % inhibition of 44.2 ± 6.5% (N = 19 independent replicates). It was therefore feasible to perform *Tc*MetRS mode inhibition studies with this compound. These studies, carried out as previously described for *Ld*MetRS, confirm a best fit to the same partial, cooperative, noncompetitive inhibition model (eq 7; Supporting Information Figure 6 and Table 4). These data show that although compound **27** inhibits *Tc*MetRS via the same mechanism as for *Ld*MetRS, the K_i of this compound is ∼5−7-fold less against the *Tc*MetRS enzyme than against *Ld*MetRS.

***Tc*MetRS: Homology Model.** To account for the different potencies observed between the *Ld*MetRS and *Tc*MetRS enzymes, *Tc*MetRS (Uniprot: Q4D6H2) was modeled on the basis of the in-house *Lm*MetRS X-ray structure cocrystallized with compound **27** (Figure 8). The sequences were 67% identical (with 81% of residue changes conservative) (Supporting Information Figure 7). Two residues that have direct contact with the ligand in the crystal structure show sequence differences between *Lm*MetRS and *Tc*MetRS. Ile418 forms nonpolar contacts with the ligand's difluorophenyl group; this interaction is reproduced by the corresponding valine residue in the *Tc*MetRS model. Phe414 forms a parallel-displaced π-stacking interaction with the pyrazolopyrimidine core in the *Ld*MetRS structure. Phe414 corresponds to an Asn in *Tc*MetRS with no accessible side-chain orientations for π-stacking with the pyrazolopyrimidine in our model. These sequence differences

https://dx.doi.org/10.1021/acsinfecdis.9b00453
ACS Infect. Dis. 2020, 6, 1044−1057

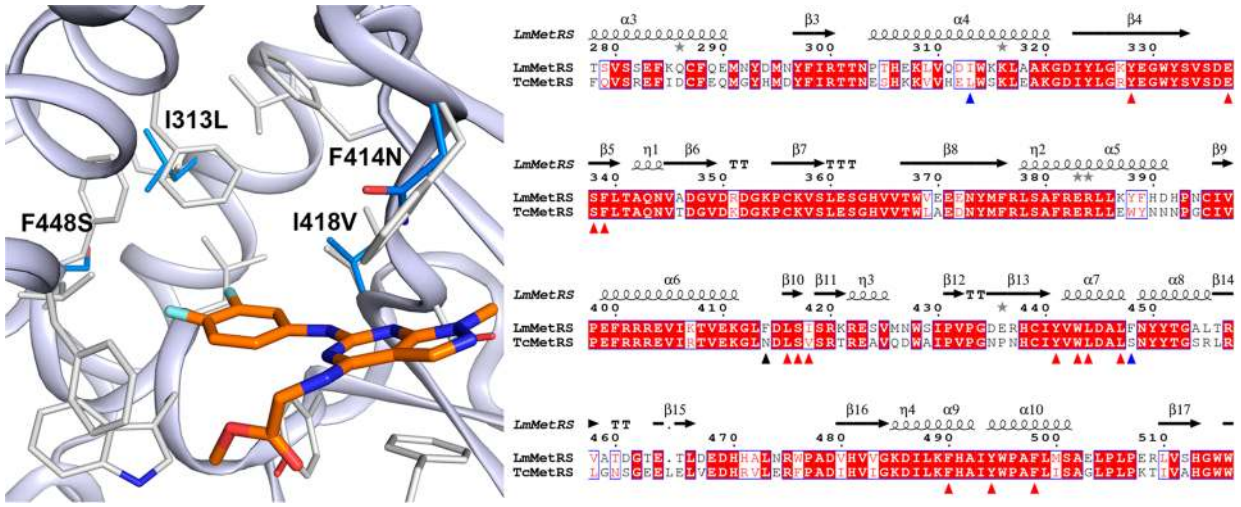

Figure 8. *Tc*MetRS homology model. Sequence differences between *Lm*MetRS and *Tc*MetRS. Superposition of *Tc*MetRS homology model on the *Lm*MetRS:Met:MetRS02 crystal structure (main chain, ribbon; side chains, gray sticks) with *Tc*MetRS sequence differences shown as sticks (C atoms, light blue) and labeled. Sequence alignment of *Lm*MetRS and *Tc*MetRS. Residues that form the MetRS02 binding site are highlighted by red upward arrows. F414N is highlighted with a black arrow, and back-pocket residues are highlighted with blue arrows.

may be an important contributor to the lower potency of the series for *Tc*MetRS compared to *Ld*MetRS.

Furthermore, Phe498 forms nonpolar contacts with the difluorophenyl group of the ligand in the crystal structure. While this is a conserved residue between the *Leishmania* and *T. cruzi* MetRS enzymes, it can adopt a distinct, flipped side-chain conformation in *Tc*MetRS and consequently may lose its contacts with the ligand. Flipping of the Phe498 side chain may be possible due to sequence differences in this region, namely, Phe448 (*Lm*) corresponding to a serine and Ile313 (*Lm*) corresponding to a leucine in *Tc*MetRS.

DISCUSSION

MetRS is a promising drug target for many disease-relevant organisms due to its central role in protein synthesis. Extensive work on this enzyme for kinetoplastid parasites *T. brucei* and *L. donovani* has focused on compounds that bind to the active site and compete with methionine, including an aminoquinolone (MetRS01) series of compounds. Despite the concerted efforts of several groups, these compounds have not progressed to late-stage drug discovery due to developability challenges (e.g., hERG liability, poor in vivo distribution, etc.). To overcome these issues there is a pressing need to identify new chemotypes that inhibit this enzyme.

In the present study, a new series of 4,6-diamino pyrazolopyrimidine (MetRS02) *Ld*MetRS inhibitors were identified following a high-throughput screen against a focused compound library enhanced with ATP mimetics. Due to the nature of the compound library screened, any hits identified were expected to compete with ATP for binding. Surprisingly, structural and enzymatic studies revealed that representative members of this compound series bind to an allosteric site not previously described and display noncompetitive inhibition where the inhibitor binds to both the free enzyme and enzyme substrate complex with equal affinity.

The identification of a novel allosteric binding pocket in the *L. donovani* and *T. cruzi* MetRS enzymes offers a new strategy from a drug discovery perspective, particularly in view of the above-mentioned challenges in development faced by existing orthosteric inhibitors. Targeting an allosteric pocket is also likely to provide new ways of achieving selectivity over human orthologues, a particular challenge for MetRS given the high degree of active site homology between kinetoplastids and human enzymes. In addition, compounds displaying non-competitive modes of inhibition are advantageous as, unlike active site inhibitors, they are not affected by high concentrations of substrates in the cell. As such, the identification of the MetRS02 compound series and binding pocket provides an opportunity to explore these allosteric inhibitors.

Within the MetRS02 series, many compounds did not achieve full inhibition of the enzyme. The level of inhibition correlates with aqueous solubility, indicating that the primary driver for the low plateaus is likely to be poor compound solubility rather than the enzyme−substrate−inhibitor complex undergoing catalysis at a reduced rate. However, in some cases, compounds with equally low solubility did achieve nearly full inhibition (e.g., **27**), whereas others (e.g., **19**) did not (Table 3). The potency and partial inhibition of these compounds correlate well with the K_i values and β-factors in Table 4, so a partial inhibition mechanism cannot be completely excluded at present. Also, it is important to point out that solubility and potency measurements are performed under different conditions (i.e., buffer composition, pH, and timing). The biochemical assay is carried out over 2 h whereas solubility is measured after 24 h to ensure that steady-state equilibrium is achieved, thus temporary supersaturation may result in compound concentrations above the reported solubility limit in the biochemical assay. Importantly, when good potency and solubility are combined, full inhibition of both the *Leishmania* and *T. cruzi* enzymes is observed (compound **31**).

Across the series, *Tc*MetRS potency was consistently lower than for the *Leishmania* enzyme, with many *Ld*MetRS active compounds inactive against the *T. cruzi* enzyme. The data for the most potent and soluble compounds indicates that the series is approximately 10-fold less potent against the *T. cruzi* enzyme. The homology model generated for *Tc*MetRS shows that some key residues involved in MetRS02 compound binding differ from those in the *Leishmania* enzyme. The Phe414 (*Lm*)/Asn (*Tc*) difference is likely a key driver for the lower effect on the *T. cruzi* enzyme. Phe414 makes an important contribution to compound binding through aromatic π-stacking with the

https://dx.doi.org/10.1021/acsinfecdis.9b00453
ACS Infect. Dis. 2020, 6, 1044−1057

pyrazolopyrimidine core which is not reproduced by the Asn residue in the *T. cruzi* enzyme. Another important difference is in the orientation of Phe498, which in the *Leishmania* structure interacts with the difluorophenyl moiety of the MetRS02 compounds. This residue is conserved in the *T. cruzi* enzyme, but our homology model predicts a different orientation for this residue, potentially precluding its contribution to ligand binding. Future chimera studies are needed to support these hypotheses.

Initial testing of selected compounds in *Leishmania* and *T. cruzi* cell-based assays showed no or minimal inhibition of parasite viability. At this stage in the development of this series, this is not surprising, as compounds are likely not potent enough to show a cellular effect and other factors such as permeability and stability may not be optimal yet. This work provides new, validated hits against *Ld*MetRS, but further improvement of the properties of the series, an understanding of the potential for selectivity over the human orthologues, and proof of concept in cell-based parasite assays are required to understand the usefulness of this new allosteric binding site in the MetRS enzyme for drug discovery purposes.

CONCLUSIONS

We have identified a novel strategy to target the essential enzyme methionyl-tRNA synthetase in kinetoplastid parasites through a newly identified allosteric pocket adjacent to the active site. Drug discovery efforts by several groups targeting the orthosteric binding site have not yielded candidates for late-stage drug discovery to date due to issues relating to poor *in vivo* distribution and hERG liability. Thus, the identification of a novel binding site and a new chemotype offers a welcome alternative to targeting this enzyme for neglected tropical diseases leishmaniasis and Chagas disease.

MATERIALS AND METHODS

***Ld*MetRS Protein Expression and Purification.** An *E. coli* codon optimized (Genscript) version of the full-length *Ld*MetRS gene (TriTrypDB ID LdBPK_210890) was cloned into the pET15b TEV vector using Nde1 and Xho1 restriction sites. The vector had been previously modified to include a His tag and a TEV cleavage site at the N terminus. The plasmid was transformed into BL21 DE3 *E. coli* cells. One liter cultures were grown in autoinduction + AMP media[28] at 37 °C and 200 rpm until the OD600 reached 0.8. The temperature was then reduced to 22 °C at 200 rpm overnight. Cells were harvested by centrifugation at 3000*g* for 20 min and stored at −20 °C. The pellets were resuspended in 150 mL of 20 mM HEPES, 500 mM NaCl, 5% glycerol, 1 mM TCEP, 10 μM $ZnCl_2$, and 20 mM imidazole pH 7.0 (buffer A) supplemented with DNase I (400 U/mL) and protease inhibitor tablets (1 per 50 mL of lysis buffer). The cells were lysed using the Continuous Flow Cell Disrupter (Constant Systems) at 30 kilo-pound per square inch. The lysate was centrifuged at 40 000*g* for 20 min, and the supernatant was then filtered (0.2 μm). The sample was loaded onto a 5 mL HiTrap His column (GE Healthcare) equilibrated with buffer A on an AKTA Purifier (GE). The column was then washed with 10 column volumes of buffer A. A step gradient of 5% buffer B (A + 500 mM imidazole) was used to remove histidine-rich protein contaminants. A gradient of 5 to 50% B over 20 column volumes was used to elute the *Ld*MetRS. The protein was then concentrated to 11 mL for gel filtration. Gel filtration was carried out on a Superdex 200 26/60 prep-grade column (GE) in 20 mM HEPES, 500 mM NaCl, 5% glycerol, 1 mM TCEP, and 10 μM $ZnCl_2$ at pH 7.0. Glycerol (10%) was added for storage at −80 °C.

***Lm*MetRS Protein Expression and Purification.** *Lm*MetRS (206−747) was expressed and purified as described previously.[26] Briefly, an *E. coli* codon optimized sequence corresponding to residues 206−747 of *L. major* MetRS (LmjF21.0810) was cloned into a pET-15-derived vector encoding an N-terminal 6xHis tag followed by a TEV cleavage site. Protein was purified by Ni-NTA affinity chromatography followed by size exclusion chromatography using 20 mM HEPES, 500 mM NaCl, 5% glycerol, 1 mM TCEP, and 10 μM $ZnCl_2$ at pH 7.0 as the buffer. Protein was concentrated to 24 mg/mL for crystallization experiments.

***Tc*MetRS Protein Expression and Purification.** The gene encoding full-length *T. cruzi* MetRS (TriTrypDB ID TcSilvio_007991) was synthesized and codon optimized for baculovirus by Genscript and cloned into pFASTBac with an N-terminal His tag and a TEV cleavage site.

The plasmid was transformed into DH10 α-cells to create the bacmid. The bacmid was then transfected into Sf9 cells in a six-well plate at 1.5×10^6 cells/well using Insect Gene Juice (Merck). The plate was incubated for 7 days at 26.5 °C. The transfection was harvested and labeled P0. The virus was then amplified sequentially to give the P1 and P2 viruses. For large-scale expression, 2×500 mL Sf9 cells at 1.5×10^6 cells/mL were infected with 3% P2 virus and incubated at 26.5 °C and 125 rpm for 72 h. Following harvesting at 1000*g* for 20 min, the cell pellet was processed immediately. For larger-scale production, expression (10L) was carried out using an Appliflex system (Applikon Biotechnology). The pellet was resuspended in 15 mL of lysis buffer per 5 g of pellet weight (25 mM HEPES pH 7.5/500 mM NaCl/2 mM DTT/5% glycerol/10 mM L-methionine/20 mM imidazole/400 U/mL DNase I/cOmplete Protease Inhibitor tablets (1 per 50 mL of lysis buffer). The suspension was then passed through a continuous flow cell disrupter (Constant Systems) at 30 kilo-pound per square inch. The sample was then centrifuged at 37 500*g* for 30 min, followed by filtration through a 0.22 μm filter.

A 5 mL His Trap Ni HP (GE Healthcare) was equilibrated with buffer A (25 mM HEPES pH 7.5/500 mM NaCl/2 mM DTT/5% glycerol/10 mM L-methionine/20 mM imidazole) on an AKTA purifier system (GE Healthcare). The sample was loaded using a sample pump at 5 mL/min. The column was then washed with 10 column volumes of buffer A. The column was then washed with 5% buffer B (25 mM HEPES pH 7.5/500 mM NaCl/2 mM DTT/5% glycerol/10 mM L-methionine/500 mM imidazole)/95% buffer A to remove contaminating histidine-rich proteins. A gradient of 5−50% buffer B was then used to elute the protein.

The protein was dialyzed against buffer C (25 mM HEPES pH 7.5/250 mM NaCl/1 mM DTT/5% glycerol/10 mM L-methionine). An XK26/60 Superdex 200 column was equilibrated with buffer C. The protein sample was concentrated to 11 mL using a 30 kDa cutoff Vivaspin spin concentrator (Sartorius), passed through a 0.22 μm filter, and loaded onto the column using a 10 mL loop at 1 mL/min. The protein, which eluted as a monomer (column calibrated with BioRAD standards), was then concentrated to 5 mg/mL. The protein was shown to be almost 100% pure by SDS-PAGE densitometry (BioRAD Imager), and the identity of the protein was confirmed by mass spectrometry.

Compound Solubility. Solubility was assessed using a filtration-based method. Test compounds were dissolved in

https://dx.doi.org/10.1021/acsinfecdis.9b00453
ACS Infect. Dis. 2020, 6, 1044−1057

DMSO to give 10 mM solutions. Five microliters of the 10 mM solution was added to 195 μL of phosphate-buffered saline at pH 7.4 and mixed for 24 h (rotary mixing, 900 rpm, 25 °C) excluding light. After mixing, the samples were filtered to remove any undissolved material using a Millipore Multiscreen HTS filter. The filtrate was analyzed for dissolved drug compounds using UHPLC.

CHI LogD and cLogP Measurements. CHI LogD measurements were performed as described elsewhere.[29] cLogP measurements were calculated using StarDrop (Optibrium).

***Lm*MetRS:MetRS02 Protein Crystallography.** Protein:ligand complexes were obtained by cocrystallization. For crystallization, *Lm*MetRS was prepared at 24 mg/mL in 20 mM HEPES, 500 mM NaCl, 0.01 mM $ZnCl_2$, 1 mM TCEP supplemented with 1 mM Mg-ATP, and 10 mM L-methionine. The ligand was solubilized to 200 mM in DMSO and added to the protein solution to a final concentration of 6 mM. Crystallization was carried out by vapor diffusion using the sitting drop method. A grid screen consisting of 23−28% PEG 3350 and 0.2 M potassium formate at pH 7.0−7.5 was prepared in 96-well MRC 2 drop plates with a reservoir volume of 50 μL. Drops were prepared by mixing 1 μL of protein with 1 μL of reservoir solution before plates were sealed and incubated at 18 °C. After 72 h, large crystals were obtained in many of the crystallization wells.

Crystals were cryoprotected in mother liquor plus 20% glycerol and flash frozen in liquid nitrogen prior to data measurement at Diamond Light Source beamline I03. Crystals were found to be isomorphous with the reported *Lm*MetRS structure belonging to the $P2_12_12_1$ space group with unit cell dimensions of a = 54.17 Å, b = 100.80 Å, and c = 132.0 Å. Diffraction data were measured to 2.0 Å resolution, integrated with XDS[30] and reduced using Aimless.[31] The structure was phased by molecular replacement as implemented in MOLREP[32] using the *Lm*MetRS:MetAMP complex (PDB 3KFL) as a search model. Refinement was carried out using Refmac5,[33] ligand topology files created with jligand[34] and manual model alteration using COOT.[35] Data measurement and refinement statistics are shown in Supporting Information Table 1. Coordinate files and associated experimental data have been deposited in the Protein Data Bank (PDB) with accession code 6SWX.

***Tc*MetRS Homology Model.** The *Tc*MetRS sequence (UniProt ID: Q4D6H2) was homology modeled on the basis of the *Lm*MetRS crystal structure with compound **27** bound using Prime Homology Modeling tools implemented in Schrödinger software (Schrödinger, LLC). Sequences were aligned using Prime ClustalW, and the model was built by applying the energy-based method, including the cocrystallized ligand. Nontemplate loops were refined in Prime (as recommended). The final model was refined in the Protein Preparation Wizard suite, and restrained energy minimization was applied to the default root-mean-square deviation of 0.3 Å.

***Tc*MetRS Assay Development and Kinetic Parameter Determinations.** The activity of the *Tc*MetRS enzyme was determined by monitoring levels of pyrophosphate released during the first step of the enzymatic reaction. The pyrophosphate formed was converted to two inorganic phosphate molecules using a pyrophosphatase enzyme, and levels of the resulting phosphate molecules were measured using the BIOMOL Green reagent (Enzo Life Sciences).

*Tc*MetRS assays were carried out using 384-well, clear, flat-bottomed plates (Greiner) at room temperature (~23 °C) in 50 μL reaction volumes of assay buffer (30 mM Tris, pH 8.0, 140 mM NaCl, 30 mM KCl, 40 mM $MgCl_2$, 0.01% (v/v) Brij-35, 1 mM DTT) plus 1 U/mL pyrophosphatase and varying concentrations of enzyme and substrates. Enzyme linearity was assessed in a 90 min end-point assay with varying *Tc*MetRS concentrations (0−320 nM), 50 μM L-methionine, and 100 μM ATP. Reactions were stopped with the addition of 50 μL of BIOMOL Green reagent, with the signal allowed to develop for 30 min before the absorbance of each well was read at 650 nm (A_{650}) using a PheraStar plate reader (BMG).

Apparent Michaelis constants (K_m^{app}) for the L-methionine and ATP substrates were determined in end-point assays using the above buffer conditions and 80 nM recombinant *Tc*MetRS. To determine L-methionine K_m^{app}, various L-methionine concentrations were tested in the presence of a fixed, saturating concentration of ATP (350 μM). To determine the ATP K_m^{app}, various ATP concentrations were tested in the presence of a fixed, saturating concentration of L-methionine (3 mM). Following a 90 min reaction at room temperature, assays were stopped with the addition of 50 μL of BIOMOL Green, and A_{650} was read as previously described. Using a BIOMOL Green phosphate standard curve, A_{650} data were converted to reaction rates and rate versus substrate concentration data were fitted to modified Michaelis−Menten equations using GraFit v6.0 (Erithacus Software). Equation 1 was used to determine the L-methionine K_m^{app}, and eq 2 was used to determine the ATP K_m^{app}.

Equation 1 (Hill equation):

$$v = \frac{V_{max}[S]^n}{K_m{}^n + [S]^n} \quad (1)$$

Equation 2 (high substrate inhibition Michaelis−Menten equation):

$$v = \frac{V_{max}}{1 + \frac{K_m}{[S]} + \frac{[S]}{K_i^s}} \quad (2)$$

v is velocity, V_{max} is the maximum velocity, [S] is the substrate concentration, K_m is the Michaelis constant, n is the Hill slope, and K_i^s is the substrate inhibition constant.

***Ld*MetRS and *Tc*MetRS Compound Screening.** All screening assays were performed in 384-well, clear, flat-bottom plates (Greiner) at room temperature (~23 °C) in 50 μL reaction volumes containing assay buffer plus 1 U/mL pyrophosphatase, 50 μM L-methionine, 100 μM ATP, and either 80 nM *Tc*MetRS or 50 nM *Ld*MetRS.

Single-point *Ld*MetRS inhibition assays were carried out by dispensing test compound (or DMSO to control wells) into assay wells using an ECHO 550 acoustic dispenser (Labcyte). Assays were then performed by adding 25 μL of assay buffer with enzyme to assay plates (with assay buffer added only to "no enzyme" control wells) before the reaction was initiated with the addition of a 25 μL mixture containing L-methionine, ATP, and pyrophosphatase to all wells. Following a 120 min reaction at room temperature, the assay was stopped with the addition of 50 μL of BIOMOL Green. The BIOMOL Green signal was allowed to develop for 30 min before the absorbance of each well was read at 650 nm using an EnVision multilabel plate reader (PerkinElmer Life Sciences) or a PheraStar plate reader (BMG). All liquid dispensing steps were carried out using a Thermo Scientific WellMate dispenser (Matrix).

https://dx.doi.org/10.1021/acsinfecdis.9b00453
ACS Infect. Dis. 2020, 6, 1044−1057

ActivityBase from IDBS (version 8.0.5.4) was used for data processing and analysis, with percentage inhibition values determined relative to 100% inhibition and 0% inhibition control wells on each plate.

To generate IC_{50} data for hit compounds in the *Ld*MetRS or *Tc*MetRS assays, 10-point inhibitor dose response curves were prepared in 384-well assay plates using an ECHO 550 acoustic dispenser (Labcyte). Following preparation of the inhibitor curves, assays were carried out as described above using either 50 nM *Ld*MetRS or 80 nM *Tc*MetRS.

ActivityBase from IDBS was again used for data processing and analysis. All IC_{50} curve fitting was undertaken using ActivityBase XE (version 7.7.1) from IDBS. A four-parameter logistic dose−response curve was utilized (XLfit model 203) with prefit used for all four parameters.

MetRS Counterscreen. Counterscreen assays, to identify any compounds inhibiting the pyrophosphatase enzyme or interfering with the BIOMOL Green assay readout, were carried out. As described above, 10-point inhibitor curves were prepared in 384-well plates using an ECHO 550 acoustic dispenser (Labcyte). Assays were performed in 50 μL reaction volumes containing assay buffer plus 1 U/mL pyrophosphatase and 1.2 μM pyrophosphate. Pyrophosphate was excluded from 100% effect control wells.

Following a 120 min incubation at room temperature (~23 °C), the detection of phosphate levels using the BIOMOL Green reagent was carried out as previously described. All liquid dispensing steps were carried out using a Thermo Scientific WellMate dispenser (Matrix).

Data processing and analysis were performed using ActivityBase from IDBS as described above.

***Ld*MetRS and *Tc*MetRS Mode of Inhibition Studies.** To establish the mode of inhibition of compounds **19** and **27**, data sets (generated using the BIOMOL Green assay platform previously described) were collected by varying both the inhibitor and substrate concentrations. Using GraFit v6.0 (Erithacus Software), each data set was globally fitted to standard competitive, uncompetitive, and noncompetitive inhibition models (eqs 3−5).

Equation 3 (competitive inhibition model):

$$v = \frac{V_{max}[S]}{K_m\left(1 + \frac{[I]}{K_i}\right) + [S]} \quad (3)$$

Equation 4 (uncompetitive inhibition model):

$$v = \frac{V_{max}[S]}{K_m + [S]\left(1 + \frac{[I]}{K_i}\right)} \quad (4)$$

Equation 5 (noncompetitive inhibition model):

$$v = \frac{V_{max}[S]}{K_m\left(\frac{1}{1 + [I]/K_i}\right) + [S]\left(\frac{1}{1 + [I]/K_i}\right)} \quad (5)$$

On the basis of poor data fits to the above models, partial inhibition and cooperativity parameters were introduced into the uncompetitive and noncompetitive models as previously described by Skovpen et al.[36,37] Mode of inhibition data were globally fitted to these modified equations (eqs 6 and 7).

Equation 6 (cooperative, uncompetitive, partial inhibition model):

$$v = \frac{V_{max}\left([S]^n + \frac{\beta[S]^n[I]^h}{K_i^h}\right)}{K_s{}^n + [S]^n + \frac{[S]^n[I]^h}{K_i^h}} \quad (6)$$

Equation 7 (cooperative, noncompetitive, partial inhibition model):

$$v = \frac{V_{max}\left(\frac{[S]^n}{K_s^n} + \frac{\beta[S]^n[I]^h}{K_s^n K_i^h}\right)}{1 + \frac{[S]^n}{K_s^n} + \frac{[I]^h}{K_i^h} + \frac{[S]^n[I]^h}{K_s^n K_i^h}} \quad (7)$$

v is the velocity, V_{max} is the maximum velocity, [S] is the substrate concentration, [I] is the inhibitor concentration, K_i is the inhibitor constant, K_s is the substrate dissociation constant, n is the substrate Hill slope, h is the inhibitor Hill slope, and β is the proportionality constant (fraction of activity remaining when the enzyme is fully saturated with inhibitor).

If more than one model appeared possible, then data were fitted to both and examined for significance using the F-test function in GraFit.

Chemistry. See the Supporting Information.

■ ASSOCIATED CONTENT

Supporting Information

The Supporting Information is available free of charge at https://pubs.acs.org/doi/10.1021/acsinfecdis.9b00453.

Summary of the *Ld*MetRS high-throughput screen; *Ld*MetRS maximum % inhibition plateau versus compound solubility; compound **27** pIC_{50} under different substrate conditions; *Ld*MetRS compound **27** mode of inhibition; *Ld*MetRS compound **19** mode of inhibition; *Tc*MetRS compound **27** mode of inhibition; sequence alignment of *Lm*MetRS and *Tc*MetRS; crystallographic data measurement and refinement statistics for *Lm*MetRS:Met:compound **27**; and chemistry experiment (PDF)

Accession Codes

Authors will release the atomic coordinates and experimental data for PDB ID code 6SWX upon article publication.

■ AUTHOR INFORMATION

Corresponding Authors

David W. Gray − *Drug Discovery Unit, Wellcome Centre for Anti-Infectives Research, School of Life Sciences, University of Dundee, Dundee DD1 5EH, U.K.*; Email: D.W.Gray@dundee.ac.uk

Manu De Rycker − *Drug Discovery Unit, Wellcome Centre for Anti-Infectives Research, School of Life Sciences, University of Dundee, Dundee DD1 5EH, U.K.*; orcid.org/0000-0002-3171-3519; Email: M.DeRycker@dundee.ac.uk

Authors

Leah S. Torrie − *Drug Discovery Unit, Wellcome Centre for Anti-Infectives Research, School of Life Sciences, University of Dundee, Dundee DD1 5EH, U.K.*

David A. Robinson − *Drug Discovery Unit, Wellcome Centre for Anti-Infectives Research, School of Life Sciences, University of Dundee, Dundee DD1 5EH, U.K.*; orcid.org/0000-0003-1979-5918

Michael G. Thomas − *Drug Discovery Unit, Wellcome Centre for Anti-Infectives Research, School of Life Sciences, University of Dundee, Dundee DD1 5EH, U.K.*

https://dx.doi.org/10.1021/acsinfecdis.9b00453
ACS Infect. Dis. 2020, 6, 1044−1057

Judith V. Hobrath − *Drug Discovery Unit, Wellcome Centre for Anti-Infectives Research, School of Life Sciences, University of Dundee, Dundee DD1 5EH, U.K.*
Sharon M. Shepherd − *Drug Discovery Unit, Wellcome Centre for Anti-Infectives Research, School of Life Sciences, University of Dundee, Dundee DD1 5EH, U.K.*
John M. Post − *Drug Discovery Unit, Wellcome Centre for Anti-Infectives Research, School of Life Sciences, University of Dundee, Dundee DD1 5EH, U.K.*
Eun-Jung Ko − *Drug Discovery Unit, Wellcome Centre for Anti-Infectives Research, School of Life Sciences, University of Dundee, Dundee DD1 5EH, U.K.*
Rafael Alves Ferreira − *Drug Discovery Unit, Wellcome Centre for Anti-Infectives Research, School of Life Sciences, University of Dundee, Dundee DD1 5EH, U.K.*
Claire J. Mackenzie − *Drug Discovery Unit, Wellcome Centre for Anti-Infectives Research, School of Life Sciences, University of Dundee, Dundee DD1 5EH, U.K.*
Karolina Wrobel − *Drug Discovery Unit, Wellcome Centre for Anti-Infectives Research, School of Life Sciences, University of Dundee, Dundee DD1 5EH, U.K.*
Darren P. Edwards − *Drug Discovery Unit, Wellcome Centre for Anti-Infectives Research, School of Life Sciences, University of Dundee, Dundee DD1 5EH, U.K.*
Ian H. Gilbert − *Drug Discovery Unit, Wellcome Centre for Anti-Infectives Research, School of Life Sciences, University of Dundee, Dundee DD1 5EH, U.K.;* orcid.org/0000-0002-5238-1314
Alan H. Fairlamb − *Drug Discovery Unit, Wellcome Centre for Anti-Infectives Research, School of Life Sciences, University of Dundee, Dundee DD1 5EH, U.K.;* orcid.org/0000-0001-5134-0329

Complete contact information is available at: https://pubs.acs.org/10.1021/acsinfecdis.9b00453

Author Contributions

L.S.T., D.A.R., M.G.T., J.V.H., E.-J.K., R.A.F., I.G.H., A.H.F., and M.D.R. conceived the work and designed experiments. L.S.T., D.A.R., M.G.T., J.V.H., S.M.S., J.M.P., E.-J.K., R.A.F., K.W., D.P.E., I.H.G., D.W.G., A.H.F., and M.D.R. performed data acquisition, analysis, or interpretation. L.S.T. and M.D.R. wrote the manuscript with contributions from D.A.R., M.G.T., J.V.H., S.M.S., E.-J.K., and D.P.E. A.H.F. carried out a substantial review of the manuscript. L.S.T., I.H.G., D.W.G., and M.D.R. performed project management and staff supervision.

Notes

The authors declare no competing financial interest.

■ ACKNOWLEDGMENTS

We acknowledge the Wellcome Trust for funding (grants 092340, 204672, and 203134). We acknowledge the support of the Drug Discovery Unit's compound management and data management teams. The authors also thank Diamond Light Source for beam time (proposal mx14980) and the staff of beamline I03 for assistance with crystal testing and data collection.

■ ABBREVIATIONS

MetRS, methionyl-tRNA synthetase; *Ld*, *Leishmania donovani*; *Lm*, *Leishmania major*; *Tc*, *Trypanosoma cruzi*; *Tb*, *Trypanosoma brucei*

■ REFERENCES

(1) Buckner, F. S., Ranade, R. M., Gillespie, J. R., Shibata, S., Hulverson, M. A., Zhang, Z., Huang, W., Choi, R., Verlinde, C., Hol, W. G. J., Ochida, A., Akao, Y., Choy, R. K. M., Van Voorhis, W. C., Arnold, S. L. M., Jumani, R. S., Huston, C. D., and Fan, E., Optimization of methionyl tRNA-synthetase inhibitors for treatment of *Cryptosporidium* infection. *Antimicrob. Agents Chemother.* 2019, *63* (4), DOI: 10.1128/AAC.02061-18.
(2) Hussain, T., Yogavel, M., and Sharma, A. (2015) Inhibition of protein synthesis and malaria parasite development by drug targeting of methionyl-tRNA synthetases. *Antimicrob. Agents Chemother. 59* (4), 1856−67.
(3) Jarvest, R. L., Berge, J. M., Berry, V., Boyd, H. F., Brown, M. J., Elder, J. S., Forrest, A. K., Fosberry, A. P., Gentry, D. R., Hibbs, M. J., Jaworski, D. D., O'Hanlon, P. J., Pope, A. J., Rittenhouse, S., Sheppard, R. J., Slater-Radosti, C., and Worby, A. (2002) Nanomolar inhibitors of *Staphylococcus aureus* methionyl tRNA synthetase with potent antibacterial activity against gram-positive pathogens. *J. Med. Chem. 45* (10), 1959−62.
(4) Ojo, K. K., Ranade, R. M., Zhang, Z., Dranow, D. M., Myers, J. B., Choi, R., Nakazawa Hewitt, S., Edwards, T. E., Davies, D. R., Lorimer, D., Boyle, S. M., Barrett, L. K., Buckner, F. S., Fan, E., and Van Voorhis, W. C. (2016) *Brucella melitensis* methionyl-tRNA synthetase (MetRS), a potential drug target for brucellosis. *PLoS One 11* (8), e0160350.
(5) Shibata, S., Gillespie, J. R., Kelley, A. M., Napuli, A. J., Zhang, Z., Kovzun, K. V., Pefley, R. M., Lam, J., Zucker, F. H., Van Voorhis, W. C., Merritt, E. A., Hol, W. G., Verlinde, C. L., Fan, E., and Buckner, F. S. (2011) Selective inhibitors of methionyl-tRNA synthetase have potent activity against *Trypanosoma brucei* infection in mice. *Antimicrob. Agents Chemother. 55* (5), 1982−9.
(6) Torrie, L. S., Brand, S., Robinson, D. A., Ko, E. J., Stojanovski, L., Simeons, F. R. C., Wyllie, S., Thomas, J., Ellis, L., Osuna-Cabello, M., Epemolu, O., Nuhs, A., Riley, J., MacLean, L., Manthri, S., Read, K. D., Gilbert, I. H., Fairlamb, A. H., and De Rycker, M. (2017) Chemical validation of methionyl-tRNA synthetase as a druggable target in *Leishmania donovani*. *ACS Infect. Dis. 3* (10), 718−727.
(7) Faghih, O., Zhang, Z., Ranade, R. M., Gillespie, J. R., Creason, S. A., Huang, W., Shibata, S., Barros-Alvarez, X., Verlinde, C., Hol, W. G. J., Fan, E., and Buckner, F. S., Development of methionyl-tRNA synthetase inhibitors as antibiotics for gram-positive bacterial infections. *Antimicrob. Agents Chemother.* 2017, *61* (11), DOI: 10.1128/AAC.00999-17.
(8) Ochsner, U. A., Bell, S. J., O'Leary, A. L., Hoang, T., Stone, K. C., Young, C. L., Critchley, I. A., and Janjic, N. (2009) Inhibitory effect of REP3123 on toxin and spore formation in *Clostridium difficile*, and *in vivo* efficacy in a hamster gastrointestinal infection model. *J. Antimicrob. Chemother. 63* (5), 964−71.
(9) Ochsner, U. A., Young, C. L., Stone, K. C., Dean, F. B., Janjic, N., and Critchley, I. A. (2005) Mode of action and biochemical characterization of REP8839, a novel inhibitor of methionyl-tRNA synthetase. *Antimicrob. Agents Chemother. 49* (10), 4253−62.
(10) Critchley, I. A., Green, L. S., Young, C. L., Bullard, J. M., Evans, R. J., Price, M., Jarvis, T. C., Guiles, J. W., Janjic, N., and Ochsner, U. A. (2009) Spectrum of activity and mode of action of REP3123, a new antibiotic to treat *Clostridium difficile* infections. *J. Antimicrob. Chemother. 63* (5), 954−63.
(11) Critchley, I. A., and Ochsner, U. A. (2008) Recent advances in the preclinical evaluation of the topical antibacterial agent REP8839. *Curr. Opin. Chem. Biol. 12* (4), 409−17.
(12) Critchley, I. A., Young, C. L., Stone, K. C., Ochsner, U. A., Guiles, J., Tarasow, T., and Janjic, N. (2005) Antibacterial activity of REP8839, a new antibiotic for topical use. *Antimicrob. Agents Chemother. 49* (10), 4247−52.
(13) Nayak, S. U., Griffiss, J. M., Blumer, J., O'Riordan, M. A., Gray, W., McKenzie, R., Jurao, R. A., An, A. T., Le, M., Bell, S. J., Ochsner, U. A., Jarvis, T. C., Janjic, N., and Zenilman, J. M., Safety, tolerability, systemic exposure, and metabolism of CRS3123, a methionyl-tRNA synthetase inhibitor developed for treatment of *Clostridium difficile*, in a

phase 1 study. *Antimicrob. Agents Chemother.* 2017, *61* (8), DOI: 10.1128/AAC.02760-16.
(14) Francklyn, C. S., and Mullen, P. (2019) Progress and challenges in aminoacyl-tRNA synthetase-based therapeutics. *J. Biol. Chem. 294* (14), 5365−5385.
(15) Lomeli, B. K., Galbraith, H., Schettler, J., Saviolakis, G. A., El-Amin, W., Osborn, B., Ravel, J., Hazleton, K., Lozupone, C. A., Evans, R. J., Bell, S. J., Ochsner, U. A., Jarvis, T. C., Baqar, S., and Janjic, N., Multiple ascending dose phase 1 clinical study of safety, tolerability and pharmacokinetics of CRS3123, a narrow spectrum agent with minimal disruption of normal gut microbiota. *Antimicrob. Agents Chemother.* 2019.
(16) Devine, W. G., Diaz-Gonzalez, R., Ceballos-Perez, G., Rojas, D., Satoh, T., Tear, W., Ranade, R. M., Barros-Alvarez, X., Hol, W. G., Buckner, F. S., Navarro, M., and Pollastri, M. P. (2017) From cells to mice to target: characterization of NEU-1053 (SB-443342) and its analogues for treatment of human African trypanosomiasis. *ACS Infect. Dis. 3* (3), 225−236.
(17) Shibata, S., Gillespie, J. R., Ranade, R. M., Koh, C. Y., Kim, J. E., Laydbak, J. U., Zucker, F. H., Hol, W. G., Verlinde, C. L., Buckner, F. S., and Fan, E. (2012) Urea-based inhibitors of *Trypanosoma brucei* methionyl-tRNA synthetase: selectivity and *in vivo* characterization. *J. Med. Chem. 55* (14), 6342−51.
(18) Zhang, Z., Koh, C. Y., Ranade, R. M., Shibata, S., Gillespie, J. R., Hulverson, M. A., Huang, W., Nguyen, J., Pendem, N., Gelb, M. H., Verlinde, C. L., Hol, W. G., Buckner, F. S., and Fan, E. (2016) 5-Fluoroimidazo[4,5-b]pyridine is a privileged fragment that conveys bioavailability to potent trypanosomal methionyl-tRNA synthetase inhibitors. *ACS Infect. Dis. 2* (6), 399−404.
(19) De Rycker, M., Baragana, B., Duce, S. L., and Gilbert, I. H. (2018) Challenges and recent progress in drug discovery for tropical diseases. *Nature 559* (7715), 498−506.
(20) Field, M. C., Horn, D., Fairlamb, A. H., Ferguson, M. A., Gray, D. W., Read, K. D., De Rycker, M., Torrie, L. S., Wyatt, P. G., Wyllie, S., and Gilbert, I. H. (2017) Anti-trypanosomatid drug discovery: an ongoing challenge and a continuing need. *Nat. Rev. Microbiol. 15* (4), 217−231.
(21) Huang, W., Zhang, Z., Barros-Alvarez, X., Koh, C. Y., Ranade, R. M., Gillespie, J. R., Creason, S. A., Shibata, S., Verlinde, C., Hol, W. G. J., Buckner, F. S., and Fan, E. (2016) Structure-guided design of novel *Trypanosoma brucei* methionyl-tRNA synthetase inhibitors. *Eur. J. Med. Chem. 124*, 1081−1092.
(22) Huang, W., Zhang, Z., Ranade, R. M., Gillespie, J. R., Barros-Alvarez, X., Creason, S. A., Shibata, S., Verlinde, C., Hol, W. G. J., Buckner, F. S., and Fan, E. (2017) Optimization of a binding fragment targeting the ″enlarged methionine pocket″ leads to potent *Trypanosoma brucei* methionyl-tRNA synthetase inhibitors. *Bioorg. Med. Chem. Lett. 27* (12), 2702−2707.
(23) Pedro-Rosa, L., Buckner, F. S., Ranade, R. M., Eberhart, C., Madoux, F., Gillespie, J. R., Koh, C. Y., Brown, S., Lohse, J., Verlinde, C. L., Fan, E., Bannister, T., Scampavia, L., Hol, W. G., Spicer, T., and Hodder, P. (2015) Identification of potent inhibitors of the *Trypanosoma brucei* methionyl-tRNA synthetase via high-throughput orthogonal screening. *J. Biomol. Screening 20* (1), 122−30.
(24) Koh, C. Y., Kim, J. E., Shibata, S., Ranade, R. M., Yu, M., Liu, J., Gillespie, J. R., Buckner, F. S., Verlinde, C. L., Fan, E., and Hol, W. G. (2012) Distinct states of methionyl-tRNA synthetase indicate inhibitor binding by conformational selection. *Structure 20* (10), 1681−91.
(25) Koh, C. Y., Kim, J. E., Wetzel, A. B., de van der Schueren, W. J., Shibata, S., Ranade, R. M., Liu, J., Zhang, Z., Gillespie, J. R., Buckner, F. S., Verlinde, C. L., Fan, E., and Hol, W. G. (2014) Structures of *Trypanosoma brucei* methionyl-tRNA synthetase with urea-based inhibitors provide guidance for drug design against sleeping sickness. *PLoS Neglected Trop. Dis. 8* (4), e2775.
(26) Larson, E. T., Kim, J. E., Zucker, F. H., Kelley, A., Mueller, N., Napuli, A. J., Verlinde, C. L., Fan, E., Buckner, F. S., Van Voorhis, W. C., Merritt, E. A., and Hol, W. G. (2011) Structure of *Leishmania major* methionyl-tRNA synthetase in complex with intermediate products methionyladenylate and pyrophosphate. *Biochimie 93* (3), 570−82.
(27) Zhang, J. H., Chung, T. D., and Oldenburg, K. R. (1999) A simple statistical parameter for use in evaluation and validation of high throughput screening assays. *J. Biomol. Screening 4* (2), 67−73.
(28) Studier, F. W. (2005) Protein production by auto-induction in high density shaking cultures. *Protein Expression Purif. 41* (1), 207−34.
(29) Thomas, M. G., De Rycker, M., Ajakane, M., Albrecht, S., Alvarez-Pedraglio, A. I., Boesche, M., Brand, S., Campbell, L., Cantizani-Perez, J., Cleghorn, L. A. T., Copley, R. C. B., Crouch, S. D., Daugan, A., Drewes, G., Ferrer, S., Ghidelli-Disse, S., Gonzalez, S., Gresham, S. L., Hill, A. P., Hindley, S. J., Lowe, R. M., MacKenzie, C. J., MacLean, L., Manthri, S., Martin, F., Miguel-Siles, J., Nguyen, V. L., Norval, S., Osuna-Cabello, M., Woodland, A., Patterson, S., Pena, I., Quesada-Campos, M. T., Reid, I. H., Revill, C., Riley, J., Ruiz-Gomez, J. R., Shishikura, Y., Simeons, F. R. C., Smith, A., Smith, V. C., Spinks, D., Stojanovski, L., Thomas, J., Thompson, S., Underwood, T., Gray, D. W., Fiandor, J. M., Gilbert, I. H., Wyatt, P. G., Read, K. D., and Miles, T. J. (2019) Identification of GSK3186899/DDD853651 as a Preclinical Development Candidate for the Treatment of Visceral Leishmaniasis. *J. Med. Chem. 62* (3), 1180−1202.
(30) Kabsch, W. (2010) Xds. *Acta Crystallogr., Sect. D: Biol. Crystallogr. 66*, 125−132.
(31) Evans, P. R., and Murshudov, G. N. (2013) How good are my data and what is the resolution? *Acta Crystallogr., Sect. D: Biol. Crystallogr. 69*, 1204−1214.
(32) Vagin, A., and Teplyakov, A. (2010) Molecular replacement with MOLREP. *Acta Crystallogr., Sect. D: Biol. Crystallogr. 66*, 22−25.
(33) Murshudov, G. N., Skubak, P., Lebedev, A. A., Pannu, N. S., et al. (2011) REFMAC5 for the refinement of macromolecular crystal structures. *Acta Crystallogr., Sect. D: Biol. Crystallogr. 67*, 355−367.
(34) Lebedev, A. A., Young, P., Isupov, M. N., Moroz, O. V., Vagin, A. A., and Murshudov, G. N. (2012) JLigand: a graphical tool for the CCP4 template-restraint library. *Acta Crystallogr., Sect. D: Biol. Crystallogr. 68*, 431−440.
(35) Emsley, P., and Cowtan, K. (2004) Coot: model-building tools for molecular graphics. *Acta Crystallogr., Sect. D: Biol. Crystallogr. 60*, 2126−2132.
(36) Skovpen, Y. V., Conly, C. J., Sanders, D. A., and Palmer, D. R. (2016) Biomimetic design results in a potent allosteric inhibitor of dihydrodipicolinate synthase from *Campylobacter jejuni*. *J. Am. Chem. Soc. 138* (6), 2014−20.
(37) Skovpen, Y. V., and Palmer, D. R. (2013) Dihydrodipicolinate synthase from *Campylobacter jejuni*: kinetic mechanism of cooperative allosteric inhibition and inhibitor-induced substrate cooperativity. *Biochemistry 52* (32), 5454−62.